

# A High Range-to-Resolution Multi-axis $\mu$ Force and Torque Sensing Platform

Bhawnath Tiwari, Mélissa Blot, Guillaume J. Laurent, Joël Agnus, Patrick Sandoz, Philippe Lutz  
and Cédric Clévy

**Abstract**—This paper presents a novel multi-axis  $\mu$ Force sensor with a range-to-resolution ratio of 55000, which makes the sensing device highly useful for wide range of applications. The presented device relies on a sensing strategy where a 2D encoded micro-pattern is encrypted to the mobile part of the compliant platform. This encoded pattern allows multi-axis visual sensing of displacements over a long range whereas Fourier computations ensures sub-pixel interpolation leading to the high resolution. The device is fabricated on a silicon wafer by means of clean room technology to comply with both precision encoding requirements and reliable mechanical behavior.

The work presents the design, modeling and fabrication as well as the experimental validation of the multi-axis  $\mu$ Force-Torque sensor. A modeling strategy is proposed for an effective estimation of force/torque with its capability to adapt non-linear stiffness evolution during the external loading. Experimentation demonstrates a sensing resolution of 2  $\mu$ N over a validated range of 110 mN. The proposed sensor measures the force along the two planar axes, and also the torque along the axis orthogonal to the plane, thus validating its axial decoupling capabilities.

## I. INTRODUCTION

**M**ICRO devices have many potential applications in both research and industries. Micro sensing devices are often used to retrieve useful local state information. Such devices present high interests in robotics or mechanical engineering as they enable to measure critical information needed to succeed in doing the desired tasks in an appropriate way (like gripping, guiding as in [1]). In the domain of mechanical properties study such as, characterization of biological cells, and fibers [2]–[4], a high-quality force sensing can efficiently benefit the characterization of different mechanical properties like stiffness, tensile strength, or different modulus. Depending on the device and application, the decision for the task handling may be done with an indirect state estimation with the help of a model [5]–[7] or based on some internal state knowledge like the case of self-sensing [8], or direct feedback from an appropriate calibrated sensor [9]. In the context of microrobotics and manipulation, the challenges raised by the fragility of the structure or the sensitivity to uneven terrain during the task handling make state estimation necessary. Especially when the environment is unknown (or changing), the sensing requirement becomes highly demanding. During the micro-manipulation and/or characterization, several phenomena (such as surface forces) becomes predominant [10], but these forces

despite their significant impact, can hardly be modeled in most of the cases. In order to address such complexity, there is requirement of early contact detection (typically few  $\mu$ N of force) but also to be able to sense force of some mN [11], which can evolve during the progress of the task. Moreover, the order of forces to be sensed may vary to several mN, as in the case of micro-assembly using glue [12], where the liquid glue can introduce capillary forces of few  $\mu$ N, but with the curing the resulted forces can go up to several mN. These kind of applications require, a high resolution in sensing for capillary forces (liquid-glue), but over a long sensing range because of the forces from curing evolution. Therefore high Range-to-Resolution ratio (RtR2) sensing is a key need for an effective handling of such tasks.

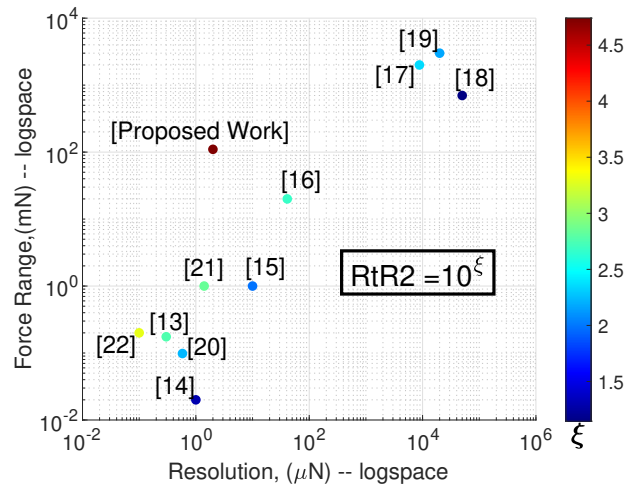


Fig. 1: Positioning of the presented work relative to the multi-axis state-of-the-art sensors

Small scale devices often have coupling behavior among different mechanical axes, and therefore for an effective study/handling of the task, multi-axis sensing is required. Several multi-axis micro-force sensors have been developed, depending on the requirements of the targeted tasks. A graphical comparison of the existing state-of-the-art multi-axis micro-force sensors [13]–[22] (similar performances along the 2 axis) with the proposed work is presented in Fig. 1. In all the cases presented in Fig. 1, the best possible sensing and range configurations are used (in case sensor has different performances under different mode of its proposed use). In Fig. 1, very few sensors are able to measure forces up to some mN range with a resolution of some  $\mu$ N. This work addresses the lock of

Authors are with FEMTO-ST Institute, Univ. of Bourgogne Franche-Comté, CNRS, F-25000 Besancon, France (e-mail: {bhawnath.tiwari, melissa.blot, guillaume.laurent, joel.agnus, patrick.sandoz, philippe.lutz, cedric.clevy}@femto-st.fr)

bringing a high RtR2 multi-axis sensing. Vision based sensing together with compliance structure constitutes a great interest in multi-axis sensing, especially when the targeted sensing need to be precise against the environmental variation, such as change of temperature, humidity. Such sensing technique can take advantage of a dedicated encoding, so as to sense over a long range and to be able to decouple different axes. The encoding strategy defined in [23] and [24] demonstrate the possibility of a precise and multi-axis sensing capability using vision. Such encoding combining together with micro-sized patterning, can help to minimize the number of pattern needed in the field of view for sensing. To use these advantages of sensing over a long range, there is requirement of a dedicated compliance structure design [25]. With the use of compliance structures, it may possible that the structure exhibit the non-linearity after some part of the linear sensing. The different force sensors discussed in the state-of-the-art, operate in linear zone with a constant value of force to displacement ratio but majority of available mechanical structures have wider non-linear zone compared to linear zone (at the micro-scale). Working in linear zone provides many advantages, such as simplified model, higher linearity, and flexibility over segment of the sensing range without knowledge of the pre-load. But, finding a way to make use of non-linear zone adds up a diverse capability to use the mechanical structure over a very high sensing range. Overall, the objective and so the key content of this work can be formulated as:

- To design a system capable of translation and rotation over a long range (corresponding to force of 100 mN or higher) and fulfilling both the encoding and mechanical requirements (section II-B).
- To develop a model which allows the use of the sensed planar positions to force and torque and is capable to adapt the force-displacement linear or non-linear relation if required (section III).
- To fabricate the corresponding structure (section IV).
- To demonstrate a high RtR2 performance experimentally (section V and VI).

The paper introduces the sensor design including its working principle and the system modeling. Then the fabrication process and experimental setup is presented followed by the experimental results validating the measurement capabilities. The paper ends with conclusion and prospects (section VII).

## II. SENSING PRINCIPLE AND PLATFORM DESIGN

### A. Sensing Principle

Force sensing is always indirect and requires physical laws and/or a model. Among the different physical principles that can be used to assess force, many limitations occur and getting a high RtR2 is really a challenge. The use of a compliant platform is a common solution and, then, force can be retrieved through the measurement of either strain, stress, displacement, etc. The force sensing principle used in this paper consists in applying the in-plane measurement method to a compliant platform of which the motion of the central part is representative of the force applied. For this purpose, a pseudoperiodic encoded pattern is encrypted on the movable

part of a compliant structure and observed by a static vision system fasten to the external structure frame. The design of a suitable compliant structure is thus required with the constraint that the encoded pattern must remain in the in-focus plane of the vision system.

### B. System Design

System design needs to fulfill a high precision requirement tied to the encoding of the platform and a sufficient mechanical flexibility to allow long range sensing. Because of the visual measurement approach chosen, the movable part must be rigid to avoid encoded pattern deformations that would result into corrupt measurements. Therefore, the mechanical structure must exhibit a movable but rigid part bound to the static frame of the structure by means of flexible links. The design should keep the advantage of symmetry and elastic behavior over a large range (to allow the best possible performance along the 2 axis). The device was fabricated through clean room processing because of precise encoding requirements (cf. Sect.II-C) and because of the highly sensitive compliant structure with beam widths of a few  $\mu\text{m}$ . The overall size of the proposed system is  $29.5 \text{ mm} \times 29.5 \text{ mm}$ , with the Central Rigid Body (CRB) of  $5.2 \text{ mm} \times 5.2 \text{ mm}$ , beams around with width of  $50 \mu\text{m}$  and thickness of  $500 \mu\text{m}$ .

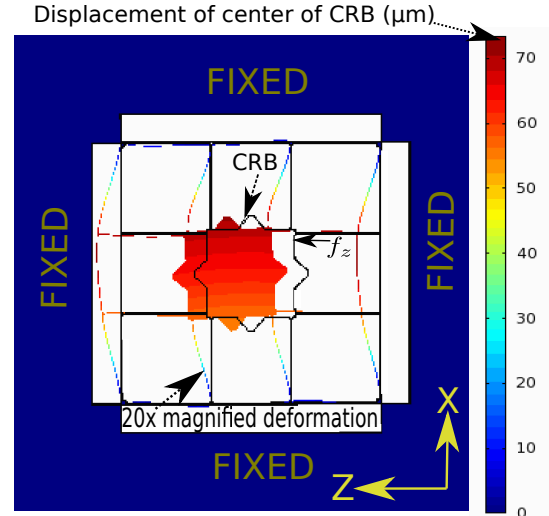


Fig. 2: Sensing platform design and working principle

Fig. 2 is a COMSOL simulation view of the sensing platform, where an external force  $f_z$  is applied, resulted into displacement of CRB, and according deformation of the beams around. The form factor of the beams ensures guided planar motion fulfilling focus requirements. The principle scheme

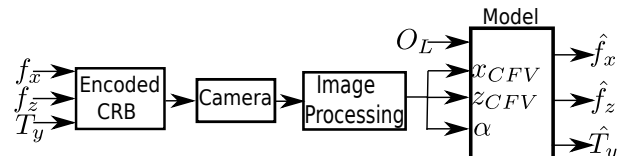


Fig. 3: Principle scheme of the force-torque sensing platform

of the platform is depicted in Fig. 3. Where  $f_x$  and  $f_z$  are respectively forces along X and Z axis, and  $T_y$  is the torque about Y,  $O_L$  is the position of the point of application of load. Vision algorithms applied to the images of the encoded pattern recorded by the camera provide three position data  $x_{CFV}$ ,  $z_{CFV}$ , and  $\alpha$ . Data  $x_{CFV}$ ,  $z_{CFV}$  refer to the X and Z positions of the center of the field of view with respect to the whole encoded pattern whereas  $\alpha$ , the angle between the pattern axes and the pixel frame axes, determines the angular position about axis Y. These data need to be used in a model so as to have an estimate of the forces ( $\hat{f}_x$ ,  $\hat{f}_z$  respectively along X and Z) and Torque ( $\hat{T}_y$  along Y). Further information on position retrieval is provided in Sect.II-C whereas Sect.III presents the platform modeling for force and torque estimation.

### C. Vision-based Position Measurement

The approach of sensing in the proposed work, consists of visual processing to retrieve data  $x_{CFV}$ ,  $z_{CFV}$  and  $\alpha$  which then need to be converted into force/torque data. This step is based on an encoded pattern of the type described in [23], [24] as well as suited decoding algorithms. Basically, the encoded pattern is made of a 2D periodic distribution of dots altered by missing lines and columns as shown in Fig. 4.

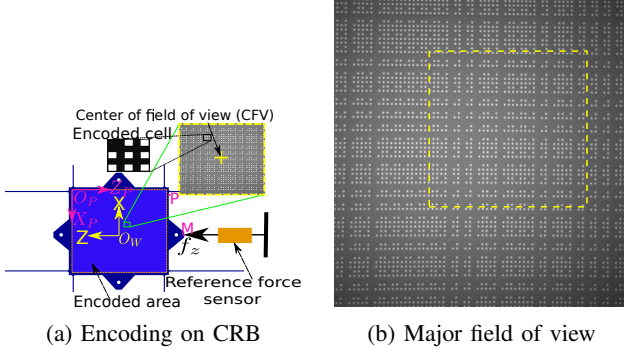


Fig. 4: Encoded Central Rigid Body (CRB)

The periodic frame allows fourier computations that result in the conversion of the pattern axes X and Z (position  $x$  and  $z$  respectively) into two linear phase maps ( $\Phi_x(x)$  and  $\Phi_z(z)$  respectively) defined by Eq. 1.

$$\begin{cases} \Phi_x(x) = 2\pi \cdot x / \lambda_{phy} \\ \Phi_z(z) = 2\pi \cdot z / \lambda_{phy} \end{cases} \quad (1)$$

where  $\lambda_{phy}$  is the physical period of the pattern. The aim of the missing lines and columns is to unequivocally break the periodicity by means of a binary code (as define in encoded cell of Fig. 4) and thus to allow the correct determination of every period index in both directions from any local view of the pattern. This is illustrated in Fig. 4 where the minor field of view of Fig. 4a is inserted in the major field of view of Fig. 4b (yellow square). Positions are retrieved for the Center of the Field of View (CFV) by involving two phase parameters as described below:

$$\begin{cases} x_{CFV} = \lambda_{phy} \frac{\phi_x}{2\pi} + k_x \lambda_{phy} \\ z_{CFV} = \lambda_{phy} \frac{\phi_z}{2\pi} + k_z \lambda_{phy} \end{cases} \quad (2)$$

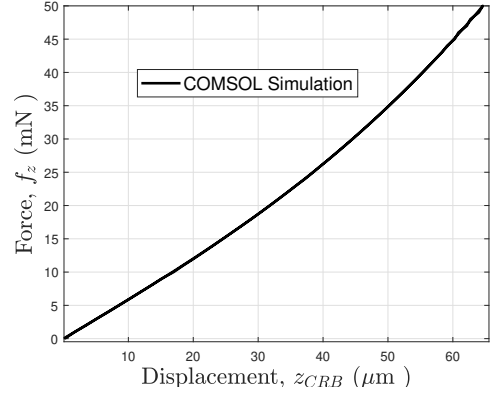


Fig. 5: System behavior from COMSOL simulation

where  $\phi_x$  and  $\phi_z$  results from the phase interpolation at the center of the field of view and  $k_x$  and  $k_z$  correspond to the correct number of entire periods. The rotation  $\alpha$  of the platform is given by the orientation of the lines and columns of dots relatively to the pixel frame of the camera.  $\alpha$  is also retrieved with a high accuracy from the phase data. In Fig. 4a,  $O_P$  is the pattern frame and  $O_W$  is the world frame. Information provided by vision algorithm is obtained originally with respect to  $O_P$  frame but, to keep the uniformity, all positions are defined throughout with respect to the world frame  $O_W$ . In practice, a physical period ( $\lambda_{phy}$ ) of  $6 \mu\text{m}$  with an encoding on 8 bits is chosen. The resulting encoded area of  $4.716 \text{ mm} \times 4.716 \text{ mm}$  is centered on the  $5.2 \text{ mm} \times 5.2 \text{ mm}$  area of the CRB.

### III. SYSTEM MODELING AND ESTIMATION

Before going for the modelling, a behavioral examination of the designed platform is carried out in COMSOL multiphysics. Because of the deformable beams around the CRB (as shown in Fig. 2), non-linearity in force-displacement relation is expected, especially when large deformation is targeted. To analyse the behavior, a ramp force of 50 mN was applied on the CRB, along the Z axis (marked as  $f_z$  in Fig. 2).

The displacement of the geometrical center of the CRB ( $z_{CRB}$ ) was retrieved from COMSOL as depicted in the force-displacement curve of Fig. 5 which shows non-linear evolution of stiffness. Any mechanical structure in general has a linear zone which may differ in size (operational region) based on the structural feature, and therefore it becomes important to have a model which could adapt to the non-linear evolution. A “Model” is presented in this work, which would basically work as a linear model for a defined linear range and as a non-linear model otherwise. If the translation along the two axes are termed as  $d_x$  and  $d_z$ , along X and Z axes respectively then overall motion along the two axes is given by Eq. 3, where  $x_I$ ,  $z_I$  are initial positions of CFV along the respective axes and  $\alpha$  is the rotation of the platform.

$$\begin{bmatrix} x_{CFV} \\ z_{CFV} \\ 1 \end{bmatrix} = \begin{bmatrix} \cos \alpha & -\sin \alpha & d_x \\ \sin \alpha & \cos \alpha & d_z \\ 0 & 0 & 1 \end{bmatrix} \begin{bmatrix} x_I \\ z_I \\ 1 \end{bmatrix} \quad (3)$$

As  $d_x$  and  $d_z$ , are pure translations, they directly depend on the forces  $f_x$  and  $f_z$  applied along these two axes. The additional displacement component (resulted from rotation) is referred to as  $P_I$  and is defined in Eq. 5.

$$\begin{bmatrix} x_{CFV} \\ z_{CFV} \\ 1 \end{bmatrix} = \begin{bmatrix} a_1 \cos \alpha & -a_1 \sin \alpha & 0 \\ a_1 \sin \alpha & a_1 \cos \alpha & 0 \\ 0 & 0 & 1 \end{bmatrix} \begin{bmatrix} \left(\frac{f_x}{a_2}\right)r_x \\ \left(\frac{f_z}{a_2}\right)r_z \\ 1 \end{bmatrix} + P_I \quad (4)$$

$$P_I = \begin{bmatrix} \cos \alpha & -\sin \alpha & 0 \\ \sin \alpha & \cos \alpha & 0 \\ 0 & 0 & 1 \end{bmatrix} \begin{bmatrix} x_I \\ z_I \\ 1 \end{bmatrix} \quad (5)$$

The overall equation including forces  $f_x$ ,  $f_z$  along the two axes and the initial position component  $P_I$  are shown in Eq. 4. The variables  $r_x$  and  $r_z$ , are representative of the linear or non-linear force-deformation relation. For instance, these variables should be unity for a linear relation and non-unity for a non-linear behavior. Depending on the material properties of the deforming structure, the non-linearity component needs to be adjusted in order to reflect the changing non-linear stiffness. Variables  $r_x$ , and  $r_z$  can be defined using Eq. 6, where def is  $x_{CFV}$  and  $z_{CFV}$  respectively for defining  $r$  as  $r_x$  and  $r_z$ .

$$r = a_3^{u(def)} \quad (6)$$

$$u(def) = \begin{cases} 0, & \text{if } 0 \leq def < d_1 \\ b_i, & \text{if } d_1 \leq def < d_{i+1} \end{cases} \quad (7)$$

Function  $u(def)$  is defined in Eq. 7 which facilitate the decision making approach by splitting the sensing range into sub-regions.  $d_i$  defines the boundaries based on the displacements. In Eq. 7, system is in linear region for  $def < d_1$ , otherwise the system is in non-linear zone.  $i$  is the number of sub-regions in non-linear zone, for  $i = 1$ , system has only 1 region (between  $d_1$  and  $d_2$ ) in non-linear zone. The force-displacement relation is defined linear for  $def < d_1$ , therefore the respective algebraic powers ( $r_x$ , and  $r_z$ ) for X and Z axis respectively must be 1 in this region. When the system is in non-linear region then the  $r_x$ , and  $r_z$  should be non-unity. But, there need to be a parameter independent of the respective algebraic powers ( $r_x$ , and  $r_z$ ), so that an adequate scaling of stiffness can be realized between linear and non-linear region. These parameters are respectively defined as  $a_1$  and  $a_2$ . The parameter required to handle  $r_x$  and  $r_z$  throughout the operational range is  $a_3$ , which is raised to zero algebraic power for linear region and non-zero positive power for non-linear. Eq. 7 defines the algebraic power of  $r_x$  and  $r_z$ , the respective intercept component in order to keep smooth computation is defined by Eq. 8. If the non-linearity component is uniform, then only one value of  $b_i$ , and  $c_i$  with  $i = 1$  is sufficient for a good force-displacement estimation. If not, the non-linear region may be divided into several sub-regions to include the changes of the non-linearity component throughout the sensing range.

$$v(def) = \begin{cases} 0, & \text{if } 0 \leq def < d_1 \\ c_i, & \text{if } d_1 \leq def < d_{i+1} \end{cases} \quad (8)$$

In order to estimate the forces and torque Eq. 4 can be inverted and written as Eq. 9 for force estimate along X and Z, where  $t_x$ , and  $t_z$  are variables defined by Eq. 10.

$$\begin{cases} \hat{f}_x = a_2 \left( \frac{t_x - v(x_{CFV})}{a_1} \right)^{\left(\frac{1}{r_x}\right)} \\ \hat{f}_z = a_2 \left( \frac{t_z - v(z_{CFV})}{a_1} \right)^{\left(\frac{1}{r_z}\right)} \end{cases} \quad (9)$$

$$\begin{bmatrix} t_x \\ t_z \\ 1 \end{bmatrix} = \begin{bmatrix} \cos \alpha & \sin \alpha & -x_I \\ -\sin \alpha & \cos \alpha & -z_I \\ 0 & 0 & 1 \end{bmatrix} \begin{bmatrix} x_{CFV} \\ z_{CFV} \\ 1 \end{bmatrix} \quad (10)$$

Considering the symmetry of the sensing platform, the mechanical parameters along X and Z axes were considered equal. Therefore the different mechanical coefficients formulated in terms of different parameters are considered same along both axes.

$$R = \sqrt{x_L^2 + z_L^2} \quad (11)$$

$$\hat{T} = f_{eq} R \sin \gamma \quad (12)$$

$$f_{eq} = \sqrt{\hat{f}_x^2 + \hat{f}_z^2} \quad (13)$$

$$\gamma = \tan^{-1} \frac{z_L}{x_L} + \tan^{-1} \frac{\hat{f}_z}{\hat{f}_x} \quad (14)$$

The torque estimation ( $\hat{T}$  can be defined by Eq. 12) requires the distance between the point of load application ( $x_L$ ,  $z_L$ ) and the center  $O_W$ , this is marked as  $R$  (Eq. 11). Where,  $f_{eq}$  (Eq. 13) is the overall force which makes an angle  $\gamma$  (Eq. 14) with frame  $O_W$ . The calculation of torque depends on the forces measured and the point of load application, and therefore the corresponding estimation accuracy is dependent on these constituents information. In the absence of any adequate commercial torque sensor, meeting both precision and workspace requirements, the current work uses the mentioned constituent information (forces measured experimentally, and point of load application) for the torque estimation.

#### IV. FABRICATION PROCESS

Use of silicon is widespread, and it enables to fabricate high aspect ratio beams. Also, its hookean nature with minimized energy dissipation and less fatigue behavior allows a high order of repeatability. Therefore silicon is chosen for the device fabrication, which started with a Silicon-on-Insulator (SOI) wafer (size 5 inch, thickness 500  $\mu\text{m}$ ) with 1.2  $\mu\text{m}$   $\text{SiO}_2$  coating on both side (Fig. 6a). One side (along with side wall) of this coating is removed with Buffered Hydrofluoric (BHF) acid etching by keeping the other side with a protective resist. The negative resist is then deposited with a designed mask, followed by resist deposition for Deep Reaction Ion Etching (DRIE). This process is done for the bottom and top side with deposition of Aluminium (electrode patterning) with the use of protective resist deposition in between. Finally, the etching of aluminium is made followed by remaining residue cleaning with acetone and ethanol respectively. As defined encoding in

Fig. 4, each square is targeted to be of  $3 \mu\text{m}$  resulting into physical period of  $6 \mu\text{m}$ . The fabrication result is shown in Fig. 6b, the obtained encoded squares on the fabricated CRB is measured  $3.01 \mu\text{m}$ , resulting into less than  $0.4 \%$  fabrication error.

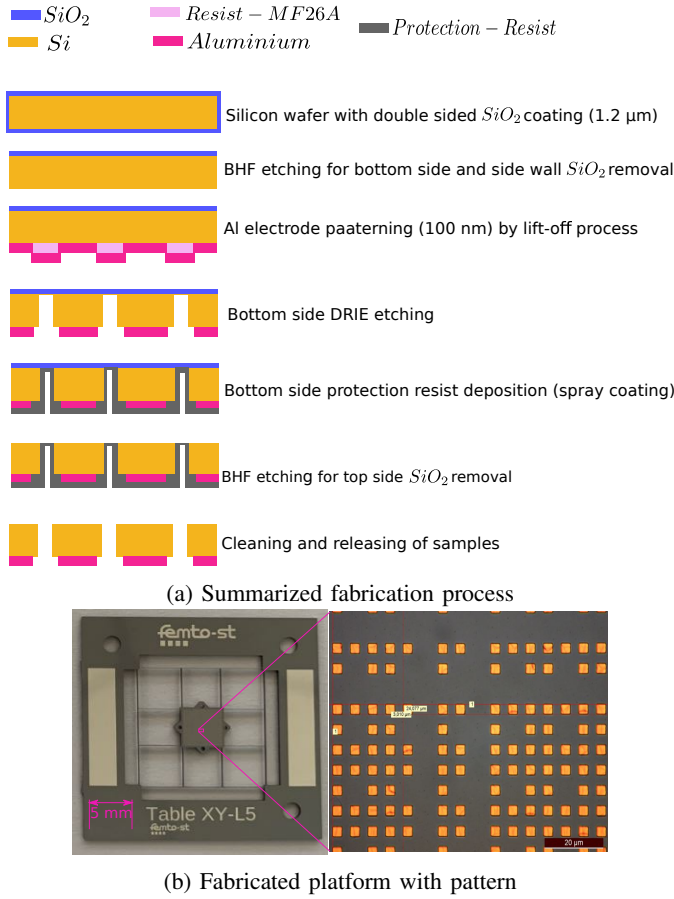


Fig. 6: Fabrication process and result

## V. EXPERIMENTAL WORKS FOR PARAMETER IDENTIFICATION

### A. Principle and Setup

The experimental validation of the model requires the knowledge of the force applied. For this purpose, the force is applied along the Z axis of the CRB by means of a reference force sensor fastened to a 1D micro-positioner. The beam deformations induced by micro-positioner displacements  $z_{Pos}$  result in displacements of the CRB which is measured by vision, and the force  $f_z$  is synchronously measured by the reference force sensor. In this way, force-displacement curves representative of the platform behavior can be recorded and used for the identification of model's parameters. The experimental setup built is shown in Fig. 7, which consists of a side view camera, a positioner, reference sensor, sensing platform and pattern monitoring camera. The sensing platform is placed with its encoded plane facing the pattern monitoring camera. A reference force sensor; either a TEI FSB-101 with a  $500 \text{ mN}$  range or a FemtoTools FT-G102 sensing finger with a  $250 \mu\text{N}$  range is used, depending on a long range validation or

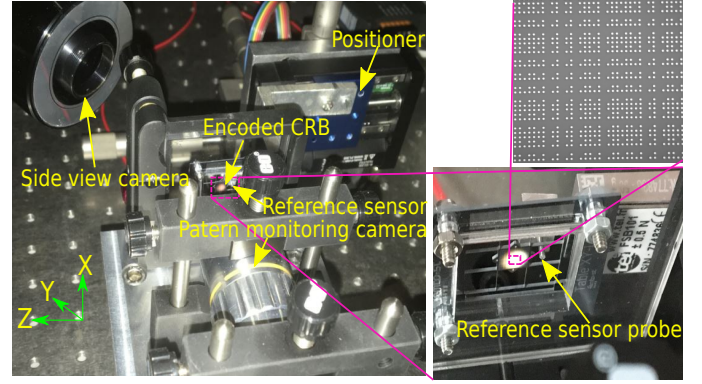


Fig. 7: Experimental setup: including the sensing platform, cameras, reference sensor and positioning stage

resolution validation requirement. The reference force sensor is attached with a M122.2DD micro-positioner from Physik Instrumente. The positioning of the reference sensor probe relatively to the platform is made with the help of a side view camera. The cameras used are IDS USB 3 uEye CP, with a  $20\times$  magnification objective from Mitutoyo integrated with OPTEM ZOOM 70 XL in the case of the pattern monitoring camera.

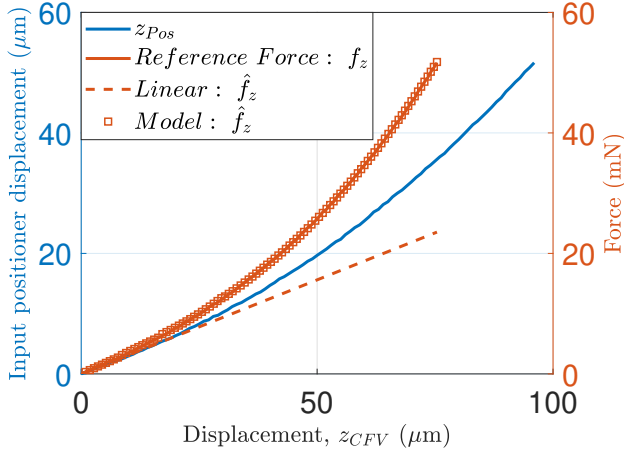
### B. Experimental Results

Fig. 8a presents the input displacement  $z_{Pos}$  (along Z) of the positioner (sampling rate of  $0.408$  samples/sec) against the resulted displacement of CFV along Z. The presence of non-linearity between input  $z_{Pos}$  and output  $z_{CFV}$  is visible because of the compliance structure. The resulting motion of the CRB is retrieved through the pattern monitoring camera and the vision algorithms. The results obtained are depicted in Fig. 8b, where the Z-X planar motion of CFV is shown, along with the rotation of the platform. The obtained motion along X and the rotation is very less compared to the force application direction (along Z).

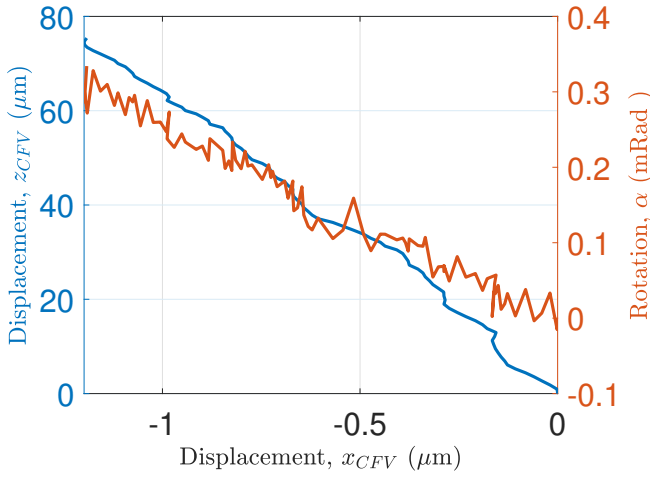
### C. Parameter Identification

The defined system parameters are identified using a non-linear least square method to fit the reference force measured. In order to minimize the non-linearity error,  $i = 5$  was chosen, resulting into splitting of operational regions into 6 sub-regions (1 linear, and 5 non-linear). The chosen boundaries of the defined sub-regions  $d_1, d_2, d_3, d_4, d_5, d_6$  are respectively  $8, 17, 30, 40, 76$  and  $115 \mu\text{m}$ . The 5 identified parameters for  $b_i$  and  $c_i$  are shown in the Table I. These parameters define the piece-wise non-linearity needed for the precise estimation of the forces. The number of parameters may be further increased to enhance the estimation accuracy, but there is a trade-off between the accuracy, number of regions and corresponding computation complexity. In the present case we opted for  $i = 5$ , as it meets the aimed within  $1 \%$  accuracy without adding complexity in the computation.

A comparison of the behavior, estimated from the model and measurements from the reference force sensor is shown in Fig. 8a. The force-displacement relation working in the



(a) Experiment for model identification



(b) Information from vision sensing

Fig. 8: Estimation from identified model, and constituent sensing from vision

TABLE I: Identified parameters (used in Eq. 4 to Eq. 9)

$i$	$a_i$	$b_i$	$c_i$
1	97.58	-0.06	0.9
2	0.034	1.2	-43.2
3	0.36	1.015	-38.67
4	-	0.992	-38.19
5	-	1.025	-37.61

linear zone ( $\text{def} < d_1$ ) if extrapolated similarly in non-linear zone then the obtained estimation ( $\hat{f}_z$ ) would be far from the true value ( $f_z$ ). This linear extrapolation plot is marked as “Linear”, whereas the defined model with inclusion of non-linearity is marked as “Model”. From the model, the estimated force ( $\hat{f}_z$ ) is very close (error less than 0.5 %) to the measurement provided by the reference force sensor ( $f_z$ ).

## VI. MODEL VALIDATION

With the defined points M and P on the CRB from Fig. 4a, additional studies of behavior are made when a force is applied at M (as for the identification) but in other case force applied at P (specific interest to study the coupling between the axis).

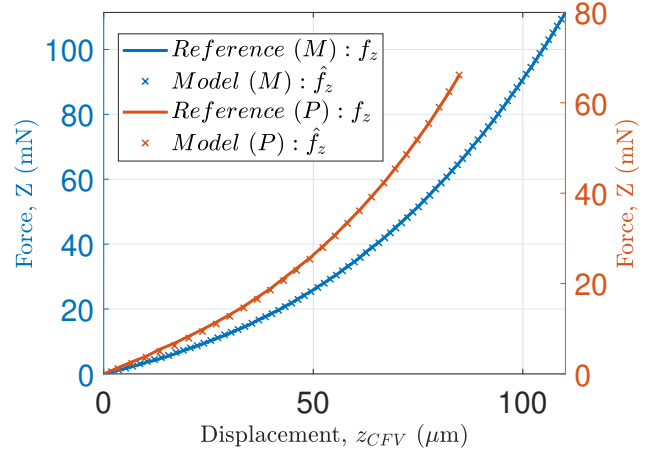


Fig. 9: Force, Z: Model Validation with force at M and P

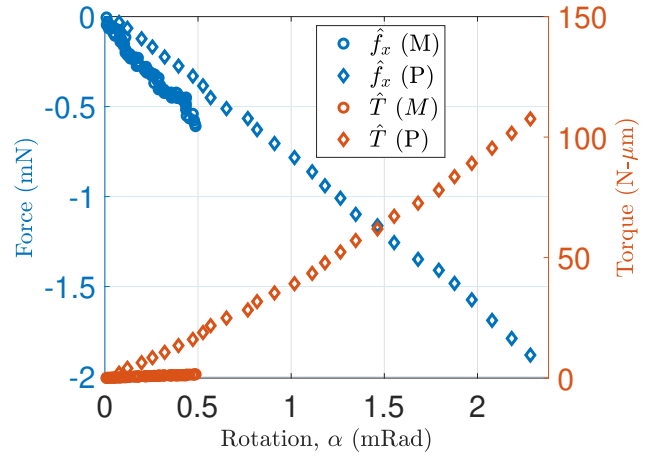


Fig. 10: Coupling: estimation of torque and force along X

With the help of the identified model, force along Z for the two cases are estimated, the estimated force in comparison to measurement from the reference force sensor is shown in Fig. 9, marked M and P for the force applied at M and P respectively. The applied force at M and P are respectively 110.2 mN and 66.1 mN. The calculated standard deviation in all the presented cases are found less than 0.35 mN, which is less than 1 % of the validated range (Fig. 12).

### A. Estimation of Torque along Y and Force along X

The coupling presence, which includes the force along X axis, and torque about the plane can be accordingly estimated from the defined model (Sect. III). Force along X is shown in Fig. 10 against the platform rotation  $\alpha$ , this represents the coupling of the two axis which is higher when the force is applied at P than M. From Eq. 4, the position of CFV is dependent on the forces applied, initial position, and the rotation of the platform. The force applied along Z at M is much higher compared to that at P (Fig. 9), but the load application at P brings the higher force along X. This mainly resulted from the beam relaxation, which is higher in case of load application closer to beams (case of P), than that at

M which is far from the supporting beams around. The extra rotation is the key factor in having higher force along the X for force at P compared to M (Eq. 9 and Eq. 10). For force at M (Fig. 9), a force of amplitude 0.6 mN is estimated along X (Fig. 10). This amplitude of force along X resulted from the maximum amplitude of 110 mN applied along Z, which is less than 1% in comparison to major sensing axis (Z). This force coming along X may not be coming from the pure coupling in sensing alone, but possible to have from axial misalignment among different constituent systems such as positioner, reference sensor, sensing platform and camera (Fig. 7). Overall, it can be said that axis decoupling is achieved within 1% of the sensing axis. For the torque estimation, from Eq. 11 to 14, the point of load application ( $x_L, z_L$ ) and the equivalent force inclination together defines the torque. The estimated torque as shown in Fig. 10, is therefore higher for load at P compared with load at M. A precise estimation of force, and the rotation can ensure an adequate estimation of the torque.

### B. Repeatability and sensing resolution validation

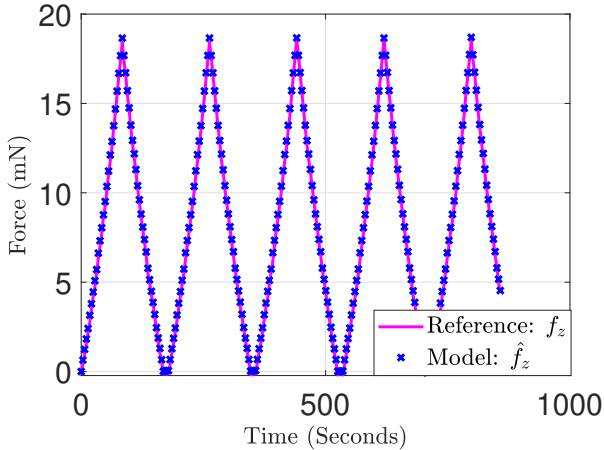


Fig. 11: Force along Z, Repeatability test

In the previous sections a long range sensing capability is demonstrated, in this subsection repeatable behavior and experimental resolution of the proposed platform is discussed. The repeatability test (Fig. 11) of the proposed force sensor is done (sampling rate of 0.166 samples/sec), the sensed deviation error is found within the proposed 1 % range, which validates high repeatability of the proposed sensing platform. The corresponding estimation errors in all the cases from identification to repetition test, are shown in Fig. 12 with an error within 1 % of sensing range.

In order to validate the high RtR2 of our proposed sensor, an experimental demonstration is needed. One required change in the experimental setup used previously, is the reference sensor with a high sensing resolution and compatible to work-space. So keeping the mentioned requirements into consideration, FemtoTools FT-G102 sensing finger is used. A staircase input of 250 nm step-size is given to the positioner. Then force from the reference sensor and positions from vision algorithm

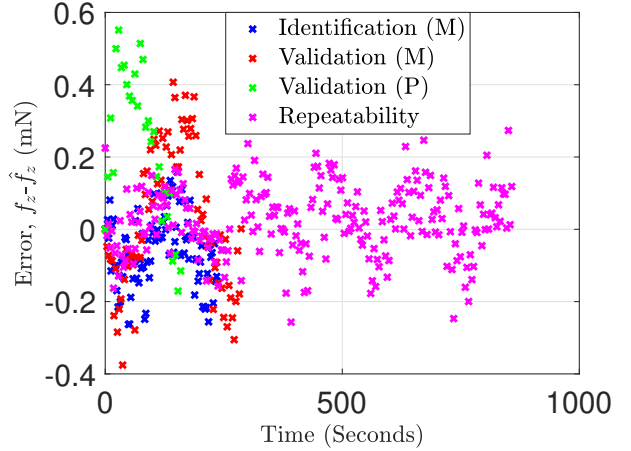


Fig. 12: Estimation error ( $f_z - \hat{f}_z$ ) from different experiments: [Identification (M)-Fig. 8a, Validation (M) and Validation (P)-Fig. 9, Repeatability-Fig. 11]

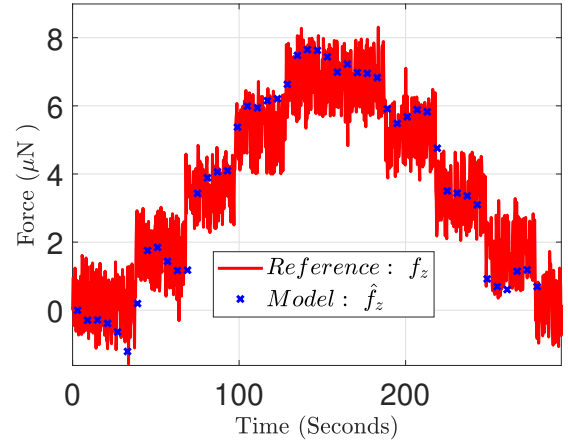


Fig. 13: Validation of resolution

were measured (sampling rate of 0.285 samples/sec). The experimental and estimation from model, are shown in Fig. 13. The obtained result estimates the force with a value close to the mean noise value of the referenced force sensor. The obtained behavior validates a sensing resolution less than 2  $\mu\text{N}$  (approximately 1.8  $\mu\text{N}$ ). Mainly this order of force brings the proposed system in linear zone, meaning that  $u(def)$  (Eq. 7),  $v(def)$  (Eq. 8) is 0. Therefore the same model, with same identified parameters is able to validate a high resolution, along with the capability to adapt non-linear regions evolution for a high range sensing.

## VII. CONCLUSIONS

This work proposes a methodology to generalize the sensing over a high range keeping advantage of linear and non-linear operational zones together. A platform capable of sensing micro-forces along 2 planar axes and torque about the plane is presented. Sensing resolution of less than 2  $\mu\text{N}$  and a force range of 110 mN are demonstrated experimentally. The estimated error and the non-linearity of the proposed sensor

are less than 1 % (better or close to the discussed state-of-the-art), but with the use of a non-linear model, a disruptive RtR2 of 55000 is successfully demonstrated. In the different micro-scale tasks, where the required forces to be sensed varies significantly with some small variation in the dependent parameters then in such cases high RtR2 force sensor becomes highly demanding. Indeed, the other use would be to use the proposed device for characterization of a wide range of devices/structures. This bolsters high acceptability of the proposed device among various tasks at micro-scale. As a future work the demonstrated force sensor may be employed in a real-time task handling.

#### ACKNOWLEDGMENT

This work was partially supported by the COLAMIR project (Contract “ANR-16-CE10-0009”), partially by the Franche-Comté region, partially by the EIPHI Graduate School (contract “ANR-17-EURE-0002”), and partially by the Robotex platform (Contract “ANR-10-EQPX-44-01”). Authors would also like to thank french RENATECH network and its FEMTO-ST technological facility.

#### REFERENCES

- [1] B. Komati, C. Clévy, and P. Lutz, “High Bandwidth Microgripper With Integrated Force Sensors and Position Estimation for the Grasp of Multistiffness Microcomponents” IEEE/ASME Trans. on Mechatronics, vol. 21, no. 4, pp. 2039-2049, 2016
- [2] M. Umashankaran and S. Gopalakrishnan, “Characterization of Bio-fiber from *Pongamiapinnata L. Bark* as Possible Reinforcement of Polymer Composites” Journal of Natural Fibers, 2019
- [3] M. W. Ullaha, M. Ul-Islam, S. Khan, Y. Kim and J. K. Park, “Structural and physico-mechanical characterization of bio-cellulose produced by a cell-free system” Elsevier, Carbohydrate Polymers 136 (2016) 908–916
- [4] V. Placet, M. Blot, T. Weemaes, H. Bernollin, G. Laurent, F. Amiot, C. Clévy and J. Beaugrand “Transverse compressive properties of natural fibers determined using micro mechatronic systems and 2D full-field measurements” Materials Today: Proceedings, 2020
- [5] F. Wang, B. Shi, Y. Tian, Z. Huo, X. Zhao, and D. Zhang, “Design of a Novel Dual-Axis Micromanipulator With an Asymmetric Compliant Structure” IEEE/ASME Trans. on Mechatronics, vol. 24, no. 2, pp. 656-665, 2019
- [6] V. Venkatesan and D. J. Cappelleri, “Path Planning and Micromanipulation Using a Learned Model” IEEE Robotics and Automation Letters, vol. 3, no. 4, pp. 3089-3096, 2018
- [7] H. Luo, W. W. Melek and J. TW Yeow, “Modelling and robust position and orientation control of a non-affine nonlinear dielectrophoresis-based micromanipulation system” Trans. of the Institute of Measurement and Control, 41(9), 2582–2595, 2019
- [8] M. Rakotondrabe, I. A. Ivan, S. Khadraoui, P. Lutz and N. Chaillat, “Simultaneous Displacement/Force Self-Sensing in Piezoelectric Actuators and Applications to Robust Control” IEEE/ASME Trans. on Mechatronics, vol. 20, no. 2, pp. 519-531, 2015
- [9] Y. Yang, J. Lou, G. Wu, Y. Wei, and L. Fu “Design and position/force control of an S-shaped MFC microgripper” Elsevier, Sensors and Actuators, vol 282, pp. 63-78, 2018
- [10] C. Clévy and M. Rakotondrabe “Microscale Specificities” Chapter 1, Signal Measurement and Estimation Techniques for Micro and Nanotechnology, Springer Science, 2011
- [11] B. Komati, K. Rabenoroso, C. Clévy and P. Lutz “Automated Guiding Task of a Flexible Micropart Using a Two-Sensing-Finger Microgripper” IEEE Trans. on Automation Science and Engineering, vol 10, no. 3, 2013
- [12] B. Tiwari, C. Clévy and P. Lutz “High-Precision Gluing Tasks Based on Thick Films of Glue and a Microrobotics Approach” IEEE Robotics and Automation Letters, vol 4, no. 4, pp. 4370-377, 2019
- [13] G. Adam and D. J. Cappelleri, “Design of a 3d vision-based micro-force sensing probe” Int. Conf. on Manipulation, Automation and Robotics at Small Scales, 2019
- [14] H. Takahashi, N. Thanh-Vinh, U. G. Jung, K. Matsumoto and I. Shimoyama, “MEMS two-axis force plate array used to measure the ground reaction forces during the running motion of an ant” Journal of Micromechanics and Microengineering 24(6):065014, 2014
- [15] M. Suzuki, T. Takahashi, and S. Aoyagi, “A Distributed 3D Force Sensor for Detecting Insect Motion by Optically Evaluating Deformation of Microscale Grid Pattern Inscribed on a Flexible Hydrogel Sheet” Int. Conf. on Solid-State Sensors, Actuators and Microsystems & Eurosensors XXXIII, 2019
- [16] X. He, J. Handa, P. Gehlbach, R. Taylor, and I. Iordachita, “A Sub-millimetric 3-DOF Force Sensing Instrument With Integrated Fiber Bragg Grating for Retinal Microsurgery” IEEE Trans. on Biomedical Engineering, vol. 61, no. 2, pp. 522-534, Feb. 2014
- [17] T. Li, N. K. K. King, and H. Ren, “Disposable FBG-Based Tridirectional Force/Torque Sensor for Aspiration Instruments in Neurosurgery” IEEE Trans. on Industrial Electronics, vol. 67, no. 4, pp. 3236-3247, 2020
- [18] A. Taghipour, A. N. Cheema, X. Gu, and F. J. Sharifi, “Temperature Independent Triaxial Force and Torque Sensor for Minimally Invasive Interventions” IEEE/ASME Trans. on Mechatronics, vol. 25, no. 1, pp. 449-459, 2020
- [19] P. Puangmali, H. Liu, L. D. Seneviratne, P. Dasgupta, and K. Althoefer, “Miniature 3-Axis Distal Force Sensor for Minimally Invasive Surgical Palpation” IEEE/ASME Trans. on Mechatronics, vol. 17, no. 4, pp. 646-656, 2012
- [20] S. Yang, Q. Xu and Z. Nan, “Design and Development of a Dual-Axis Force Sensing MEMS Microgripper” Journal of Mechanism and Robotics, 9(6): 061011, 2017
- [21] F. Beyeler, S. Muntwyler and B. J. Nelson, “A Six-Axis MEMS Force–Torque Sensor With Micro-Newton and Nano-Newtonmeter Resolution” Journal of Microelectromechanical Systems, vol. 18, no.2, 2009
- [22] S. Muntwyler, F. Beyeler and B. J. Nelson, “Three-axis micro-force sensor with sub-micro-Newton measurement uncertainty and tunable force range” Journal of Micromechanics and Microengineering, 20(2010)
- [23] Antoine N. André, P. Sandoz, B. Mauzé, M. Jacquot, and G. J. Laurent, “Sensing One Nanometer over Ten Centimeters: A Micro-Encoded Target for Visual In-Plane Position Measurement” IEEE/ASME Transactions on Mechatronics, vol. 25, no. 3, pp. 1193-1201, 2020
- [24] Antoine N. André, P. Sandoz, B. Mauzé, M. Jacquot, and G. J. Laurent, “Robust phase-based decoding of absolute (X, Y,  $\theta$ ) positioning by vision” IEEE Trans. on Instrumentation and Measurement, vol. 70, pp. 1-12, 2021
- [25] Y. K. Yong, S. S. Aphale, and S. O. R. Moheimani, “Design, Identification, and Control of a Flexure-Based XY Stage for Fast Nanoscale Positioning” IEEE Trans. on Nanotechnology, vol. 8, no. 1, 2009

**Bhawnath Tiwari** received the B.Tech degree from the Madan Mohan Malaviya University of Technology, Gorakhpur, India, in 2015 and M.S. degree in complex system engineering from University of Technology of Compiègne in 2017. He is currently working toward the PhD degree in automatic control at the University of Franche-Comté, Besançon, France. His research interests include mechatronics system design, their modeling, instrumentation, fabrication and control.



**Mélissa Blot** received the engineering degree, in 2018, from ENSMM (Ecole Nationale Supérieure de Mécanique et des Microtechniques), in Besançon, France. She worked as a research engineer in the Automatic Control and Micro-Mechatronic Systems Department (AS2M) of the Femto-ST Institute. Her research interests include development of micro-force sensors.





**Guillaume J. Laurent** received the Ph.D. degree in control systems and computer sciences from the University of Franche-Comté, Besançon, France, in 2002. He is currently an Associate Professor with the National School of Mechanics and Microtechnologies (ENSMM), Besançon. He is a member of the Automatic Control and Micro-Mechatronic Systems Department, FEMTO-ST Institute. His research interests include microrobotics, vision, parallel, and continuum robots.



**Cédric Clévy** received his Ph. D. degree in Automatic Control and computer Sciences in 2005 from the University of Franche-Comté, France. Since 2006, he has been an Associate Professor at the University of Bourgogne Franche-Comté, Besançon, France working in the AS2M (Automatic Control and MicroMechatronic Systems) department of FEMTO-ST Institute. His research interests are the design, modeling and control of micro and nanorobotic systems for the characterisation, manipulation and assembly at micro and nanoscales. Cédric

Clévy currently leads the "Micro and Nano Robotics" research team of the FEMTO-ST Institute and co-leads the thematic research group "multiscale manipulation" of the Robotics Group of Research from the CNRS - National Research Center. He is also an active member of the IEEE/RAS technical committee for "Micro/Nano Robotics and Automation" and currently serving as Associate Editor for IEEE T-ASE and Technical Editor for IEEE/ASME T-Mech.



**Joël Agnus** received the Master of Science in Electrical Engineering in 1994 and the Ph.D degree in Automatic Control and Computer Sciences from the University of Besançon, France, in 2003. He is a research engineer at ENSMM engineering school and FEMTO-ST / AS2M department. He is involved in microrobotics field, and more particular concerning microgrippers, piezoelectric material and piezoresistive force sensors within micromanipulation domain and for surface characterization applications



**Patrick Sandoz** received the Ph.D. degree in engineering science from the University of Franche-Comté, Besançon, France, in 1993. He is currently a Senior Researcher with CNRS, French National Center for Scientific Research, and a member of the Applied Mechanics Department, FEMTO-ST Institute, Besançon. His research interests include optical instrumentation and measurements and their applications.



**Philippe Lutz** is Professor at the University of Franche-Comté, Besançon, since 2002. He was the head of the research group "Automated Systems for Micromanipulation and Micro-assembly" of the AS2M department of FEMTO-ST Institute from 2005 to 2011. He was the Director of the PhD graduate school of Engineering science and Microsystems with more than 400 PhD students from 2011 to February 2017, and he is currently the head of the Doctoral College. Since January 2017, he is the director of the AS2M Research department of

FEMTO-ST. His research activities at FEMTO-ST are focused on the design and control of micro-nano systems, microgrippers, micro-nano robots, feeding systems and micro-nano manipulation, assembly stations, and Optimal design and control of piezoelectrically actuated compliant structures. P. Lutz received several awards of IEEE, authored over 90 refereed publications (50 in high standard journals), serves as associate editor for the IEEE T-ASE and as Technical Editor for the IEEE/ASME T-Mech, is member of several steering committees and is member of the IEEE Robotics and Automation Society (RAS) Committee on Micro-Nano Robotics.